

EFFECT OF MOLTING ON THE AERODYNAMIC CHARACTERISTICS OF BLACK-TAILED GULLS

Yoshiharu TANAHASHI[1], Fumihide SAKAI[1], Souta NISHIZUKA[1], Tadashige IKEDA[1], Naoko KISHIMOTO[2], Masato TAMAYAMA[3], Yasuko IWAMI[4] & Naoki TOMITA[4]

[1] Chubu University
[2] Kwansei Gakuin University
[3] Japan Aerospace Exploration Agency
[4] Yamashina Institute for Ornithology

Abstract

Birds undergo a seasonal biological process called "molting," where worn flight feathers are replaced in a specific sequence after the breeding season. During this phase, birds must operate with partially missing wing surfaces, resulting in a state of flight with localized wing defects. To clarify the aerodynamic impact of these wing defects, this study conducted comprehensive low-speed wind tunnel tests using high-precision 3D-printed models and numerical fluid dynamics analysis based on 3D CAD data. The results indicated that while the global lift and drag coefficients showed no significant differences between the feathered and unfeathered configurations, the rolling moment coefficient exhibited distinct and clear changes when a geometric defect existed exclusively on a single wing. This paper explicitly focuses on the aerodynamic influence of partial wing defects on the rolling moment characteristics, providing a detailed comparison between experimental and numerical flow fields to further clarify these phenomena.

Keywords: Aerodynamic characteristics, Molting, Black-tailed gull, Internal balance sensor, Surface pressure distribution

1. Introduction

Natural flyer systems, particularly migratory and soaring birds, exhibit unparalleled aerodynamic efficiency, adaptability, and robust multi-axis flight control capabilities that surpass current small-scale unmanned aerial vehicles (UAVs). Avian wings serve simultaneously as lifting surfaces, propulsion mechanisms, and multi-axis control effectors through continuous, active shape morphing. However, these highly optimized bio-structures are subject to severe environmental and physiological constraints. Among these, the phenomenon of "molting" represents a critical phase in the life cycle of virtually all avian species [1].

Following the breeding season, birds systematically shed old, worn flight feathers—specifically the primary and secondary remiges—and grow new ones in a tightly regulated sequential order to maintain a baseline level of flight functionality [1]. This biological necessity implies that for a significant duration of the year, known as the molting period, birds are forced to operate in environments with structurally compromised, asymmetric, and discontinuous wing geometries [2].

Despite the physical gaps in their wings, field observations confirm that birds such as wild Black-tailed Gulls continue to execute demanding aerial maneuvers, forage over long distances, and complete seasonal migrations [1]. From an engineering perspective, this introduces a fascinating paradox: how do birds mitigate the aerodynamic penalties of localized wing defects, and what are the specific fluid mechanical consequences of asymmetric wing defects on multi-axis stability? Understanding these mechanisms not only illuminates the evolutionary adaptations of avian flight but also provides valuable bio-inspired insights into the fault-tolerant control of aircraft experiencing sudden structural damage or morphing wing configurations.

Extensive research has been dedicated to the kinematics and aerodynamics of bird flight, focusing on flapping wing flight, gliding efficiency, and the role of flexible feathers in preventing stall. Traditional ornithological studies have qualitatively evaluated the energetic costs of molting, noting increases in metabolic rates and temporary reductions in escape performance. In the domain of fluid dynamics, previous international efforts have established fundamental baselines for avian configurations. Notably, initial wind tunnel testing programs evaluated the complex aerodynamic parameters of taxidermy bird models, including both the Black-tailed Gull (*Larus crassirostris*) and the Black Kite (*Milvus migrans*) [5, 6]. These studies identified critical challenges associated with the structural elasticity (deformation) of soft, real-feather biological specimens under high aerodynamic loads, motivating the transition toward rigid, non-deformable geometric representations [7].

Building upon these foundations, Takahashi et al. (2025) achieved a substantial advancement by evaluating the multi-axis aerodynamic characteristics of a rigid Black-tailed Gull model [7]. They established that the down-twisted wing geometry yields a gradual expansion of the upper-surface separation zone, which prevents sudden stall. They also elucidated crosswind characteristics, identifying that the rolling moment trends under strong and gentle breezes are highly dependent on the three-dimensional gull-wing dihedral profile [7].

However, quantitative investigations that systematically isolate all six components of aerodynamic forces and moments acting on an authentic avian body with discrete, localized feather defects remain scarce. Most existing aerodynamic models assume perfect bilateral symmetry, thereby neglecting the complex cross-coupling effects induced by single-wing feather shedding. Consequently, the precise fluid dynamic interaction between asymmetric chordwise defects, regional surface pressure generation, and multi-axis torque characteristics has not been fully established.

To bridge these research gaps, this study presents a comprehensive experimental and numerical investigation into the aerodynamic characteristics of the Black-tailed Gull (*Larus crassirostris*) during its molting phase [1, 2]. Utilizing high-fidelity three-dimensional (3D) printed models and advanced computational fluid dynamics (CFD), we systematically evaluate the complete set of aerodynamic parameters consisting of the three forces—lift (C_L), drag (C_D), side force (C_Y)—and the three moments—pitching (C_m), rolling (C_l), and yawing (C_n) [1].

The primary objective of this paper is to demonstrate that the aerodynamic penalties associated with localized feather defects are highly isolated rather than globally destructive [2]. We establish that while global longitudinal force coefficients track closely with the fully feathered baseline configuration (Normal), a highly localized and pronounced asymmetry is restricted to the lateral-directional components, particularly the rolling moment [1, 2].

Crucially, this paper refines and corrects previous hypotheses regarding flow mechanisms by leveraging the computational framework validated by Takahashi et al. (2025) [7]: we demonstrate that while large-scale spatial flow separation and stall vortices are prominent at an extreme angle of attack (30 degrees), they do not constitute the primary driver of aerodynamic divergence within the standard operational envelope. Instead, the phenomenon is governed by highly localized shifts in the upper and lower surface pressure distributions directly within and around the defect zone [2]. Furthermore, we validate an elegant attitude restoration strategy, illustrating how birds can easily and completely neutralize this asymmetric rolling torque by adjusting their aerodynamic sideslip angle, thereby achieving stable trim equilibrium with minimal energetic expenditure [2].

2. Experimental Setup and Aerodynamic Framework

The baseline geometric profile of an adult Black-tailed Gull was captured and reconstructed using high-resolution 3D CAD software, ensuring authentic reproduction of the camber, twist distribution, and wing-body blending features characteristic of the species, following the geometric parameters defined in Takahashi et al. (2025) [7]. The reference model representing the fully feathered, pristine, and symmetric state is designated as the Normal (nor) configuration [1, 2]. The model possesses a total wingspan (b) of 1200 mm and a characteristic body length of 300 mm [1, 2].

To replicate the structural gaps that arise during the sequential shedding of primary flight feathers, two distinct unfeathered configurations were engineered by removing specific chordwise sections exclusively from the left wing lifting surface, thereby establishing a controlled state of lateral asymmetry [1, 2]:

- P1L Configuration (Inner Defected): This model simulates the shedding of the inner primary feathers [1, 2]. The defect is positioned relatively close to the wing-root/mid-span junction, centered at a distance of approximately 340 mm from the body centerline, with an isolated defect area of roughly 860 mm² (Figure 1) [1, 2].
- P10L Configuration (Outer Defected): This model simulates the shedding of the outer primary feathers near the wingtip [1, 2]. The defect is located at a distance of approximately 550 mm from the centerline, featuring a larger removed area of approximately 2100 mm² due to the elongated nature of distal primary feathers (Figure 2) [1, 2].

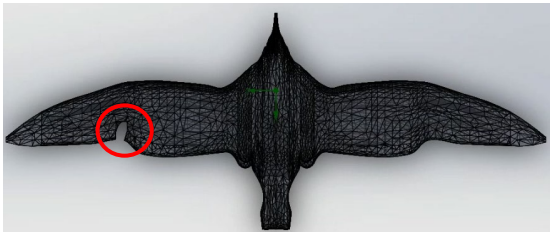


Figure 1 –Model with the inner defected when viewed from above（P1L)

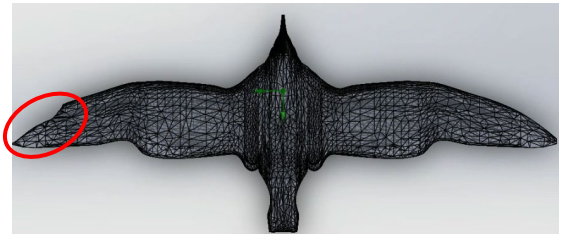


Figure 2 –Model with the outer defected when viewed from above（P10L)

In both modified models, the right wing remains completely intact and fully feathered, providing a direct internal baseline for asymmetric lift generation [1, 2]. The models were manufactured using an industrial-grade high-precision 3D printing system to ensure surface smoothness and strict adherence to the CAD coordinates (Figure 3) [2].

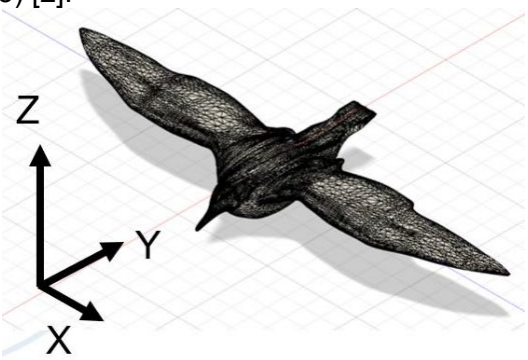


Figure 3 –Coordinate system of the CAD coordinates

All experimental trials were executed in the specialized low-speed wind tunnel facility housed within the Japan Aerospace Exploration Agency (JAXA) [2]. The wind tunnel operates under a closed-loop layout capable of delivering highly uniform flow fields with low turbulence intensity. To minimize aerodynamic interference from external mountings and capture the pure aerodynamic forces acting on the gull geometry, a high-precision, low-noise 6-axis force & moment sensor (manufactured by Leptrino Co., Ltd.) was rigidly integrated internally within the core of the 3D-printed model fuselage [2].

The internal balance sensor was directly grounded to the main vertical support strut assembly. Because the balance is fully enclosed inside the model's physical boundary, the external aerodynamic drag, lift, and side forces acting on the exposed vertical support strut do not enter the structural load path of the internal sensor crystal elements. Therefore, no external tare correction or mathematical subtraction of the strut's aerodynamic force profile was necessary.

The free-stream velocity within the test section was maintained at a constant 10 m/s for all data-acquisition runs [1, 2]. Based on the mean aerodynamic chord (MAC=0.146m) of the wing, the operational Reynolds number was fixed at approximately 9.80×10^4, which closely mirrors the natural gliding and soaring regimes of the Black-tailed Gull (*Larus crassirostris*) in coastal wind currents [7].

To ensure the absolute accuracy of the multi-axis load measurements, a rigorous signal conditioning

and cross-talk decoupling protocol was enforced. The multi-channel raw voltage outputs from the internal 6-axis balance were processed using a calibrated "cross-axis interference matrix". This decoupling process mathematically eliminates electrical and mechanical cross-talk among the orthogonal force and moment channels, ensuring that high lifting forces do not induce false rolling or yawing signals.

To eliminate static gravitational tares, internal structural tension, and geometric alignment offsets, the pure aerodynamic force vector was isolated by calculating the exact difference between the blowing condition (onwind) and the wind-off zero-velocity condition (nowind) at each specific angle of attack (Eq. (1)):

Force&Moment (pure aerodynamic) = *Force&Moment* (onwind) – *Force&Moment* (nowind) (1)

$$C_L = \frac{2F_z}{\rho SU^2},\ C_D = \frac{2F_y}{\rho SU^2},\ C_Y = \frac{2F_x}{\rho SU^2},\ C_m = \frac{2M_x}{\rho SU^2 MAC},\ C_l = \frac{2M_y}{\rho SU^2 b},\ C_n = \frac{2M_z}{\rho SU^2 b} \quad (2)$$

Here, the orientation of the 6-axis force & moment sensor corresponds to the CAD coordinate system, but the center of rotation is located at the center of the fuselage. The direction of the moment is defined as positive according to the right-hand rule for each axis. To filter high-frequency aerodynamic noise and unsteady wake fluctuations, the data streams were smoothed using a continuous 200-point moving average [1, 2]. The non-dimensional aerodynamic coefficients were defined using standard aerospace formulations, where ρ= 1.225 kg/m^3 represents the air density, S = 0.175 m^2 represents the reference wing area, and b = 1.2 m represents the full wingspan (Eq. (2)) [1, 2].

Furthermore, to eliminate minor structural, geometric, or manufacturing asymmetries inherent to the 3D-printing and mounting process, a "comparative delta analysis (difference analysis)" was introduced for the lateral-directional components. The side force (C_Y), rolling moment (C_l), and yawing moment (C_n) profiles for the unfeathered states are plotted exclusively as the exact mathematical difference relative to the symmetric Normal baseline configuration (Eq. (3)):

ΔC_Y = C_Y (defect) – C_Y (nor), ΔC_l = C_l (defect) – C_l (nor), ΔC_n = C_n (defect) – C_n (nor) (3)

This delta isolation framework guarantees that any remaining background symmetry deviations are subtracted out, leaving the pure, isolated aerodynamic signature induced solely by the feather defect [2].

3. Numerical Simulation Methodology and Validation

Numerical simulations were performed to provide high-resolution flow-field visualization and surface pressure data using SOLIDWORKS Flow Simulation [1, 2]. The software solves the Reynolds-Averaged Navier-Stokes (RANS) equations governing three-dimensional, incompressible, viscous fluid flow [3]. To model turbulence effects accurately within the boundary layer and separated shear regions without excessive computational overhead, the solver utilizes a modified k-ε turbulence model [3, 4].

Crucially, as substantiated by Takahashi et al. (2025), this solver incorporates an advanced Enhanced Wall Function approach based on the Two-Scale Wall Functions framework [7]. This mathematical formulation automatically switches between a logarithmic velocity profile in well-developed turbulent boundary layers and a laminar sublayer formulation in areas of low Reynolds numbers or approaching flow separation [3, 4]. This specific configuration is highly effective at capturing localized shear layer detachment and boundary layer transitions over complex cambered geometries, making it uniquely qualified for evaluating avian wing surfaces [7].

The computational domain was extended extensively in all directions—upstream, downstream, laterally, and vertically—to prevent artificial blockage effects and boundary reflections from corrupting the solution field [3]. The absolute boundaries were designated as follows: the inlet boundary was located 3 body lengths upstream of the model nose, the outlet boundary was located 7 body lengths downstream of the wing trailing edge to allow full wake development, and the lateral/vertical walls were positioned 4 wingspans away from the model center.

The boundary conditions were configured to replicate the wind tunnel test section environment [2]:

- Inlet Boundary: Specified as a uniform velocity inlet with v = 10 m/s along the longitudinal axis,

with a low ambient turbulence intensity of 0.1% [2].

- Outlet Boundary: Configured as a static pressure outlet set to normal atmospheric conditions (101,325 Pa) [2].
- Model Surfaces: Defined as rigid, no-slip adiabatic walls with standard aerodynamic roughness [3].
- Domain External Walls: Configured as slip walls to simulate unconfined external atmospheric conditions [4].

The angle of attack was swept continuously across a broad operational spectrum ranging from -30 up to +30 degrees to comprehensively chart both linear lifting performance and deep-stall regimes [1, 2].

To ensure numerical accuracy and grid independence, a rigorous grid convergence study was conducted based on the meshing protocols validated in Takahashi et al (2025) [7]. The solver utilizes a rectangular Cartesian mesh system, where cells intersecting the solid geometry are automatically split into polyhedral cut-cells [3, 4].

The grid density optimization sequence was structured into three specific density classifications: a Coarse Mesh containing approximately 115,000 cells, a Medium Mesh containing 268,000 cells, and a Fine Mesh containing 425,565 cells [2]. The Coarse Mesh failed to capture the thin boundary layer over the down-twisted wingtips, resulting in an underprediction of the lift-curve slope. The Fine Mesh layout (425,565 cells) was achieved by applying multi-level local refinements: Level 3 refinement patches were mapped to the leading edge to resolve the stagnation point, and Level 4 local refinement nesting was enforced inside and surrounding the geometric boundaries of the P1L and P10L defect cavities [2]. This optimized grid density achieved complete stabilization of the force residuals and matched the experimental lift and drag data within the experimental error margins across the linear flight envelope, cementing the validity of the numerical framework [7].

4. Aerodynamic Component Comparison and Results

To fully evaluate the aerodynamic consequences of molting, the six non-dimensional coefficients were analyzed [1, 2]. In accordance with the analytical strategy, global longitudinal forces and the pitching moment are evaluated through direct coefficient matching across the configurations [1]. Conversely, the lateral-directional components are evaluated strictly within the comparative delta framework to isolate the asymmetric signatures (Figure 4, 5) [2].

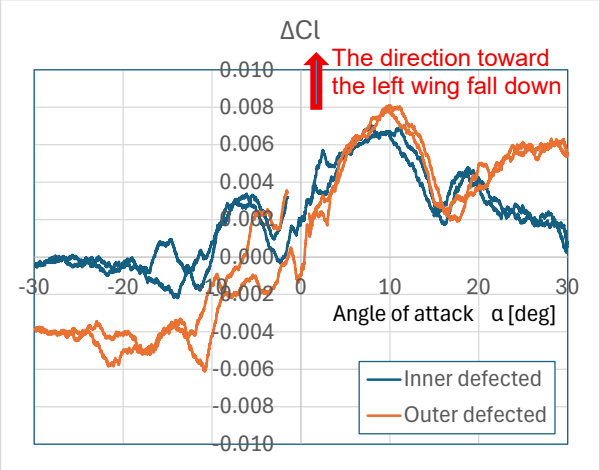


Figure 4 – Rolling moment coefficients as a function of angle of attack (measurement)

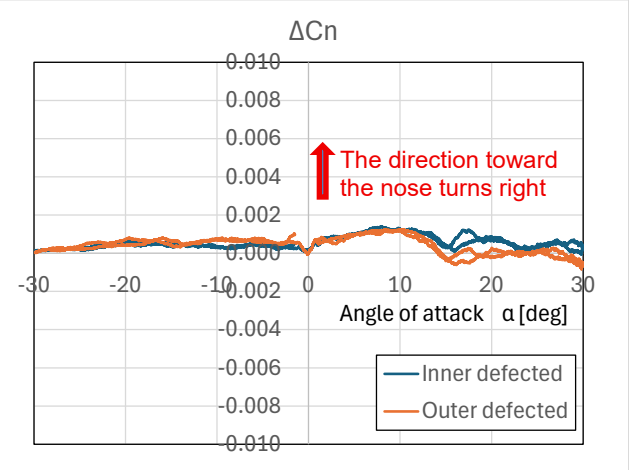


Figure 5 – Yawing moment coefficients as a function of angle of attack (measurement)

The direct comparison of global force coefficients reveals an exceptionally high degree of congruence among the Normal, P1L, and P10L configurations [1]. This tracking proves that the total force output of the wing system is largely immune to small, localized feather losses [1].

Across the entire range of angles of attack, the lift coefficient curves for both the proximal (P1L) and distal (P10L) defect models lie completely on top of the Normal baseline model [1]. No early stall onset, severe loss of maximum lift, or shift in the lift-curve slope is observed [1]. The down-twisted wing

geometry of the Black-tailed Gull inherently distributes the lifting load such that a localized gap does not trigger a catastrophic global lift deficiency [7].

Similarly, the drag coefficient tracks identically across all three configurations [1]. The profile drag at zero lift and the induced drag penalty at high lift coefficients show no observable elevation in the defect states [1]. The localized removal of primary feathers does not generate massive parasitic drag penalties or wake disruption capable of increasing total resistance [1].

Longitudinal trim and pitching stability are dictated by the pitching moment coefficient curve [1]. The experimental and numerical data reveal that the longitudinal center of pressure is stable and unaffected by the unfeathered wing state [1]. The pitching moment curves show a negative, stable slope that matches perfectly among the Normal, P1L, and P10L models [1]. At a representative nominal glide angle of attack, the absolute coefficient values are virtually indistinguishable across all configurations, displaying a high level of mathematical congruence [1]. This minute variation confirms that the longitudinal aerodynamic balance is fully preserved during molting, meaning the bird requires no additional longitudinal elevator trim or tail plane adjustments to maintain its pitch attitude (Figure 6) [1].

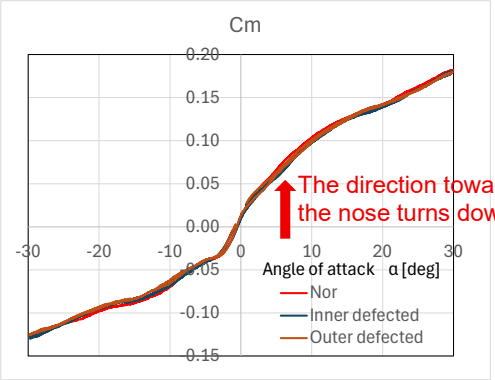


Figure 6 – Pitching moment coefficients as a function of angle of attack (measurement)

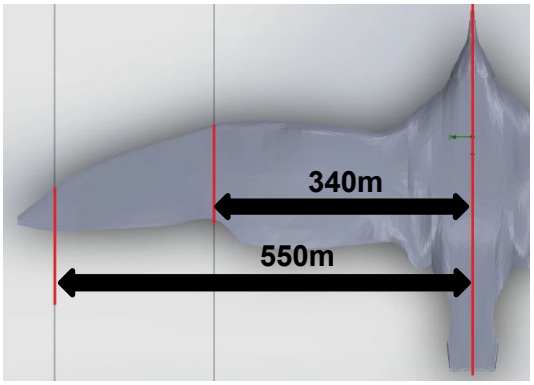


Figure 7 – Distance from the center of the model to the evaluated cross-sections

In sharp and profound contrast to the longitudinal components, the lateral-directional components evaluated within the comparative delta framework (Normal-subtraction analysis) exhibit an immediate and highly visible divergence from the symmetric baseline, revealing the exact aerodynamic cost of single-wing feather shedding [2]. Under perfectly symmetric flow conditions, an ideally balanced avian body should generate zero lateral force and zero asymmetric moments. However, when the background values are isolated via the subtraction framework, a distinct hierarchy of molting impact emerges [2].

At a representative nominal glide angle of attack, both the P1L and P10L configurations demonstrate a clear, positive rolling moment delta [2]. This positive rolling moment signifies a distinct aerodynamic torque that rolls the bird toward the defective left side (left wing drop), directly caused by the geometric asymmetry [1, 2]. Concurrently, the directional yawing moment delta also register positive shifts across the unfeathered configurations [2].

Crucially, comparative analysis reveals that the magnitude of and the directional yawing moment delta is roughly an order of magnitude smaller than the primary rolling moment delta across the operational envelope [2]. This behavior explicitly proves that the global aerodynamic penalty of asymmetric molting is overwhelmingly isolated within the single rolling axis, while lateral drift and directional yawing divergence remain minor and easily manageable [2].

5. Discussion and Physical Mechanisms

To clarify the underlying physical mechanisms governing how the wing defect configuration influences the rolling moment, we perform a high-resolution localized analysis of the numerical flow-field streamlines, velocity distributions, and surface pressure profiles [1, 2].

When analyzing the internal cross-sectional streamlines and velocity contours passing directly through

the defect zones, distinct variations in the flow patterns and flow separation behaviors can be observed depending on the specific defect location (Figure 7~9) [1]. However, when examining the upper and lower surface pressure contour fields within the low-to-moderate angle of attack range typical of stable flight (from -10 to +10 degrees), there are no globally massive or visually prominent differences in the overall pressure field across the main wing surfaces [2]. This indicates that the global flow remains primarily attached and stable within this linear flight envelope [2].

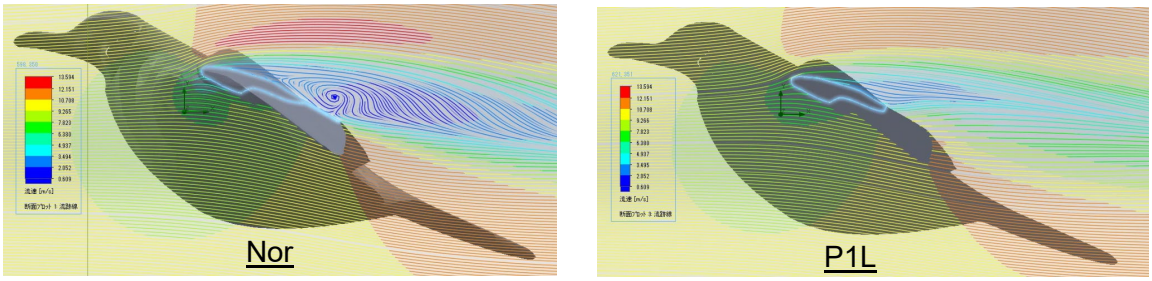


Figure 8 – Flow path lines and velocity 340 mm from the center at the angle of attack 30 degrees.

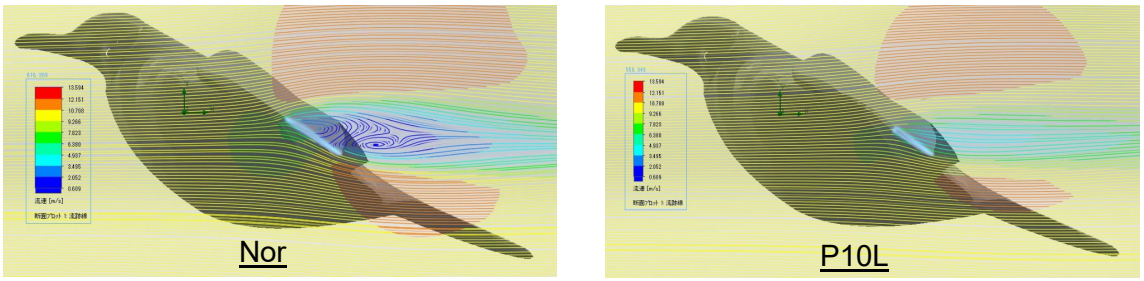
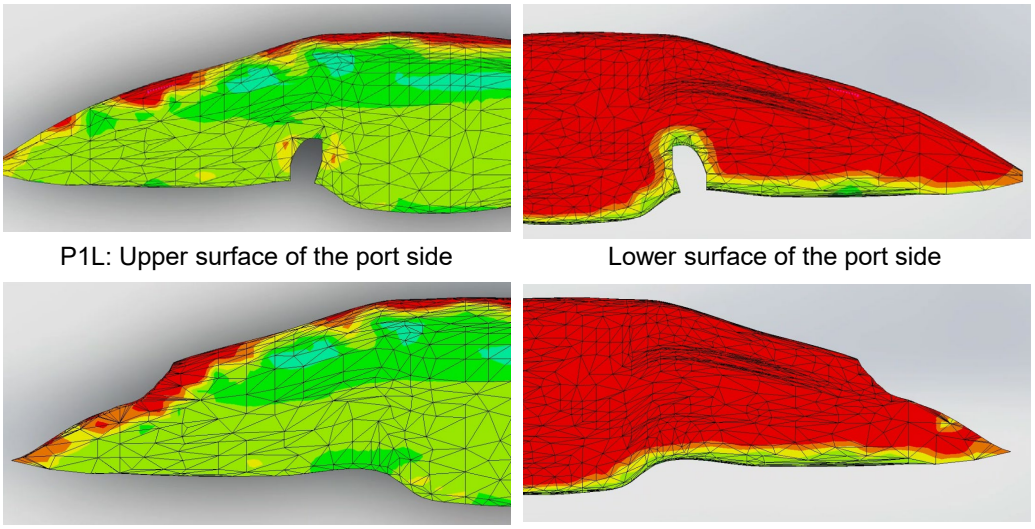


Figure 9 – Flow path lines and velocity 550 mm from the center at the angle of attack 30 degrees.

Instead, the fundamental driver of the rolling moment generation is revealed through a highly localized, precise comparison of the surface pressure distributions directly in the immediate vicinity of the defect zones [1, 2].

When the local surface pressure contours are examined closely, a distinct asymmetry between the left and right wings is observed (Figure 10, 11) [1, 2]:

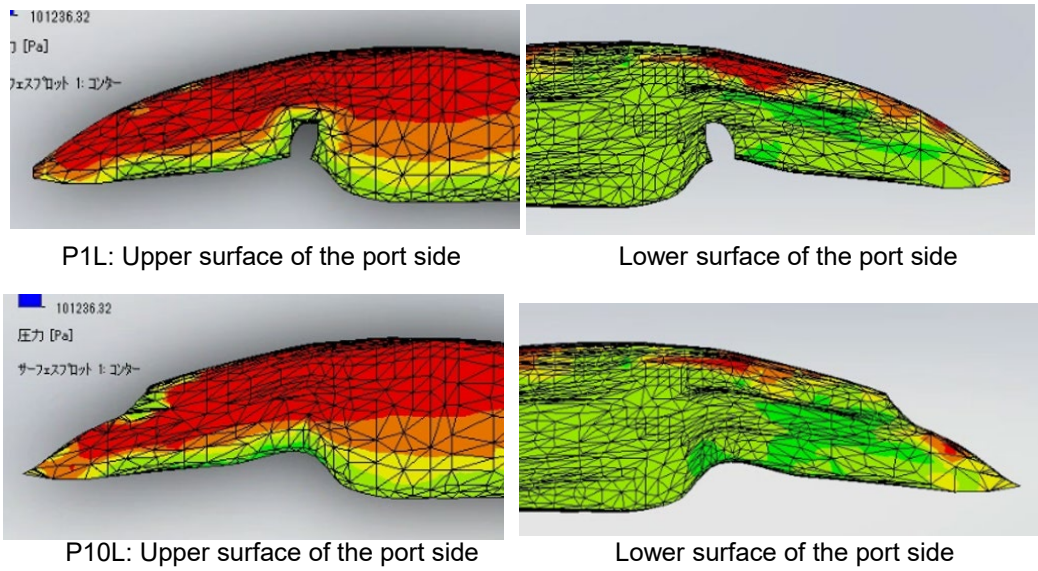


P1L: Upper surface of the port side | Lower surface of the port side

P10L: Upper surface of the port side | Lower surface of the port side

* Warm colors indicate areas of high pressure, while cool colors indicate areas of low pressure.

Figure 10 – Pressure contours at the angle of attack 30 degrees



P1L: Upper surface of the port side | Lower surface of the port side

P10L: Upper surface of the port side | Lower surface of the port side

* Warm colors indicate areas of high pressure, while cool colors indicate areas of low pressure.

Figure 11 – Pressure contours at the angle of attack -30 degrees

1. **Upper Surface Pressure Increase (Weakened Suction)**: On the upper wing surface, the static pressure in the localized zone directly surrounding the left wing defect cavity is distinctly higher than that of the corresponding pristine, fully feathered right wing surface [1, 2]. This localized pressure elevation demonstrates that the physical removal of the wing chord section weakens the suction (negative pressure) field normally generated on the upper lifting surface [1, 2].
2. **Lower Surface Pressure Decrease**: Conversely, on the lower wing surface, the local static pressure directly beneath the left wing defect zone exhibits a distinct drop, showing lower absolute values compared to the pristine right wing lower surface [1, 2].
3. **Reduction of the Upper-to-Lower Pressure Delta**: As a direct thermodynamic consequence of this concurrent upper-surface pressure increase and lower-surface pressure decrease, the net pressure difference between the upper and lower surfaces narrows significantly and compresses within the defect section [1, 2]

This localized narrowing of the upper-to-lower surface pressure difference leads directly to a substantial regional drop in the section lift over that specific spanwise section [1, 2]. Because the intact right wing continues to generate its full, uncompromised lift profile while the defective left wing suffers this localized drop in section lift, a distinctly asymmetric lift distribution is established across the wingspan [2]. This severe spanwise lift imbalance generates the net rolling couple that continuously acts to roll the avian body downward toward the unfeathered left side (left wing drop) [1, 2].

Furthermore, the absolute magnitude of the resulting rolling moment for the P1L and P10L configurations is demonstrated to be primarily dictated by the geometric distance of the defect zone from the aircraft's spanwise centerline [1, 2]. The distal defect (P10L), located farther outboard near the wingtip, operates with a significantly longer moment arm than the proximal defect (P1L), thereby exercising a more pronounced leverage on the rolling torque characteristics [1, 2].

To counter this rolling moment imbalance and prevent roll attitude divergence, a molting bird must employ an active aerodynamic stabilization strategy [2]. Our parametric analysis over a range of sideslip angles establishes that the rolling moment characteristics can be effectively controlled and adjusted [2]. While the fully feathered Normal configuration maintains a well-balanced rolling moment coefficient of approximately zero at zero sideslip, the unfeathered P1L and P10L configurations experience a continuous rolling torque under symmetric conditions [2].

Crucially, the experimental and numerical data reveal that by actively introducing and adjusting the aerodynamic sideslip angle, the bird can completely suppress and eliminate the asymmetric rolling moment [2]. The lateral cross-flow coupling generates a counter-acting rolling torque that effectively neutralizes the lift deficit of the left wing, restoring the net rolling moment back to an ideal trimmed equilibrium [2]. This confirms that adjusting the sideslip attitude serves as a highly practical, low-energy flight control strategy utilized by birds to preserve balance and maintain stable trajectories despite structural single-wing defects during the molting season [2].

6. Conclusions

This study evaluated the aerodynamic consequences of molting on the Black-tailed Gull (*Larus crassirostris*) through low-speed wind tunnel testing utilizing an internally mounted 6-axis balance and numerical fluid dynamics simulations [1, 2, 7]. The major conclusions are summarized below:

1. **Aerodynamic Performance Isolation**: Global longitudinal force components, including total lift and drag, as well as the pitching moment, exhibit near-identical profiles with negligible variations when comparing feathered and unfeathered configurations [1]. The global lifting efficiency and longitudinal trim remain completely unimpaired during molting [1].
2. **Pronounced Rolling Asymmetry in Delta Profiles**: When evaluated within the comparative Normal-subtraction delta framework using cross-talk decoupled onwind - nowind data, the presence of a single-wing defect generates an immediate divergence in the rolling moment delta, producing a roll torque toward the unfeathered left side [2]. The corresponding side force and directional yawing moment delta remain minor, confirming that the aerodynamic penalty is overwhelmingly isolated within the roll axis [2].
3. **Pressure-Driven Primary Mechanism**: High-resolution CFD demonstrates that while spatial flow separation occurs at an extreme angle of attack (30 degrees), it is not the primary driver of aerodynamic divergence within the standard flight envelope [2]. Instead, the rolling imbalance is dictated by highly localized surface pressure alterations within the defect cavity [1, 2]. The geometric gap increases upper-surface static pressure and decreases lower-surface pressure, narrowing the local upper-to-lower pressure difference and degrading regional lift production [2].
4. **Effortless Flight Restoration Strategy**: The bird can counteract this molting-induced rolling torque by optimizing its aerodynamic sideslip angle [2]. Exploiting the lateral cross-coupling derivative, a small intentional sideslip angle neutralizes the roll asymmetry, allowing the Black-tailed Gull to restore balance and execute steady flight tracks with minimal energetic expenditure despite structural wing defects [2].

7. Contact Author Email Address

mailto: tanahashi@fsc.chubu.ac.jp

8. Copyright Statement

The authors confirm that they, and/or their company or organization, hold copyright on all of the original material included in this paper. The authors also confirm that they have obtained permission, from the copyright holder of any third party material included in this paper, to publish it as part of their paper. The authors confirm that they give permission, or have obtained permission from the copyright holder of this paper, for the publication and distribution of this paper as part of the ICAS proceedings or as individual off-prints from the proceedings.

References

[1] Nishizuka S. The title of the conference paper. *Proc Investigation of Aerodynamic Characteristics of Black-tailed Gulls during Molting*, Chubu University, Vol. 1, No. 1, pp 1–45, 2024.

[2] Sakai F. The title of the conference paper. *Proc Investigation of Rolling Moment Characteristics of Black-tailed Gulls during Molting*, Chubu University, Vol. 1, No. 1, pp 1–52, 2025.

[3] Hachinohe T, Jones B and Brown J. *Getting started with stress, thermal, and fluid simulation using SOLIDWORKS: An introduction to SOLIDWORKS Simulation/Flow Simulation*. 1st edition, Morikita Publishing Co., Ltd., 2019.

[4] Shinohara M. *CAE classroom using SOLIDWORKS: Mechanism analysis/fluid analysis*. 1st edition, Corona Publishing Co., Ltd., 2022.

[5] Kishimoto N, Wada D, Tamayama M, Iwami Y, Tomita N, Ikeda T, Tanahashi Y and Katagiri K. Wind tunnel experiment of taxidermy black-tailed gull (Larus crassirostris) and black kite (Milvus migrans). *Proc 33rd Congress of the International Council of the Aeronautical Sciences (ICAS 2022)*, Stockholm, Sweden, Vol. 1, Paper ICAS-2022-0814, pp 1–12, 2022.

[6] Kishimoto N, Wada D, Tamayama M, Iwami Y, Tomita N, Ikeda T, Tanahashi Y and Katagiri K. Evaluation of wind tunnel test results of taxidermy black-tailed gull (Larus crassirostris). *Proc 34th*

Congress of the International Council of the Aeronautical Sciences (ICAS 2024), Florence, Italy, Vol. 1, Paper ICAS-2024-0549, pp 1–10, 2024.

[7] Takahashi Y, Tanahashi Y, Ikeda T, Kishimoto N, Wada D, Tamayama M, Iwami Y and Tomita N. Wind tunnel modeling and investigation of aerodynamic characteristics of black-tailed gull. *Transactions of the Japan Society for Aeronautical and Space Sciences*, Vol. 68, No. 6, pp 224–231, 2025.